Cell-imaging probe

DOI: 10.1002/smll.200700457

High-Contrast Paramagnetic Fluorescent Mesoporous Silica Nanorods as a Multifunctional Cell-Imaging Probe**

*Chih-Pin Tsai, Yann Hung, Yi-Hsin Chou, Dong-Ming Huang, Jong-Kai Hsiao, Chen Chang, Yao-Chang Chen, and Chung-Yuan Mou**

Cells have many advantages as therapeutic agents. They are able to carry out complex functions, as in stem cell[1] or immune cell therapy.[2] For effective therapy, the delivered cells must carry long-lived tracking agents for monitoring the position and fate of the injected cells. At present, monitoring is often carried out by slow histological analysis, which requires tissue biopsy. Recently, the development of noninvasive real-time tracking of injected cells has attracted a lot of attention for its clinical potential. Fluorescent nanomaterials have been successfully utilized as labels in biological and medical applications for imaging[3,4] and diagnostic purposes.[5–7] The limited capability of the fluorescence technique in detecting deep tissues restricts the collection of information in vivo. Magnetic resonance imaging (MRI), one of the most important noninvasive imaging techniques, has been widely used for clinical diagnosis[8] and biomedical research. However, its sensitivity is relatively low for cellular-level applications.[9] Hence, the synthesis of a new MRI contrast agent[10–13] with high sensitivity would be of great interest.

Recently, the development of a nanomaterial-based probe with multifunctionalities has become a very active field. Preferably, the functionalities should combine the advantages of MRI in noninvasiveness, fluorescence in high sensitivity and resolution, a surface functional group for targeting, and the ability to deliver drugs locally. Among these, the carrying of good and long-lived MRI contrast agents would be the most useful. Our interest is in developing a nanoparticle form of mesoporous silica, which has some unique properties, such as rigid structure, large pore volume, uniform pore size, great surface-modification capability,[14] and good biocompatibility. It has also been demonstrated as a biomarker[15,16] and a drug carrier.[17–19] Previously, we reported multimodal tumblerlike mesoporous silica, which carries a magnetic iron oxide nanoparticle as a T_2 contrast agent (T_1 and T_2 = magnetic relaxation times) and a fluorescent dye.[20] However, the T_2 agent often gives poor contrast in dark areas, such as the liver. Herein, we report a new multifunctional mesoporous silica nanorod that possesses green fluorescence and paramagnetism, and could serve as a good contrast agent in T_1 and T_2 imaging.

The multimodality of nanoparticle-based monitoring agents has been developed before. However, very few have been demonstrated as a platform in cell monitoring.[21] There are several different combinations of luminescent materials, MRI contrast agents, and support. The iron oxide nanoparticle, a typical T_2 contrast agent, has been demonstrated to be a multimodal probe by surface functionalization with Cy5.5 dye and chlorotoxin to detect gliomas.[22] Santra and co-workers also developed novel multifunctional probes by encapsulating Gd-TSPETE (n-trimethoxysilylpropyl)ethyldiamine triacetic acid trisodium salt) and CdSe:Mn/ZnS core–shell quantum dots or Gd-TSPETE and $[Ru(bpy)_3]^{2+}$ (bpy = 2,2′-bipyridine) in a silica matrix.[23,24] Both hybrid silica nanoparticles increase the transverse relaxation rate ($1/T_2$) more than the longitudinal relaxation rate ($1/T_1$), and function better as T_2 contrast agents. The development of a multifunctional agent with T_1-weighted imaging enhancement is thus desirable and some have been reported recently; for example, quantum dots coated with paramagnetic PEGylated lipid[25] (PEG = polyethylene glycol) and Gd-DTTA-modified (DTTA: diethylenetriaminetetraacetate) silica spheres doped with $[Ru(bpy)_3]^{2+}$.[26]

The multifunctional nanorods were synthesized by surfactant-templated self-assembly under basic conditions (Scheme 1). We prepared a solution by dissolving cetyltrimethylammonium bromide (CTAB; 0.58 g) and an ethanol solution (0.2 M, 5 mL) of tetraethyl orthosilicate (TEOS) in $NH_4OH_{(aq)}$ (0.5 M), and the mixture was stirred at 50°C for 5 h. Then an aqueous solution (2.5 mL) of *N*-1-(3-trimethoxysilylpropyl)-*N*-2-(diethylenetriaminepentaacetic acid) phenylthiourea (DTPA-ph-NCS-APTMS), an ethanol solution (2.5 mL) of *N*-1-(3-trimethoxysilylpropyl)-*N*-fluoresceinylthiourea (FITC-APTMS), both prepared in advance, and an ethanol solution (1.1 M, 5 mL) of TEOS were added sequentially with vigorous stirring. The mixture turned turbid in 1 min and was stirred for 1 h followed by aging at 50°C for

[*] C.-P. Tsai, Dr. Y. Hung, Prof. C.-Y. Mou
Department of Chemistry
National Taiwan University
1 Roosevelt Rd., Sec. 4, Taipei 106 (Taiwan)
Fax: (+886) 2-2366-0954
E-mail: cymou@ntu.edu.tw
Y.-H. Chou, Dr. C. Chang
Institute of Biomedical Science (IBMS)
Academia Sinica
128 Academia Rd., Sec. 2, Nankang, Taipei 115 (Taiwan)
Dr. D.-M. Huang
Center for Nanomedicine Research
National Health Research Institutes
35 Keyan Rd., Zhunan Town, Miaoli County 350 (Taiwan)
Dr. J.-K. Hsiao
Department of Medical Imaging
National Taiwan University Hospital and College of Medicine
1 Jen-Ai Rd., Sec. 1, Taipei (Taiwan)
Dr. Y.-C. Chen
Department of Laboratory Medicine
National Taiwan University Hospital and College of Medicine
1 Jen-Ai Rd., Sec. 1, Taipei (Taiwan)

[**] This work was supported by a grant from the National Research Council, Taiwan. We thank Miss Chao-Yu Chen for the confocal microscopy measurements.

Supporting Information is available on the WWW under http://www.small-journal.com or from the author.

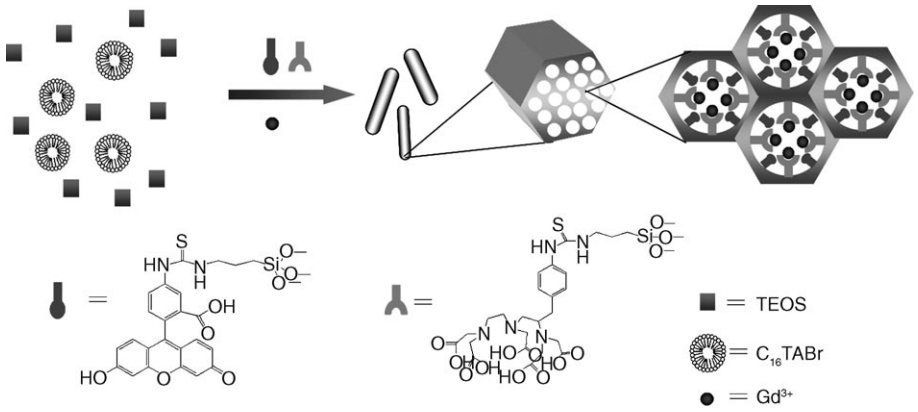

Scheme 1. Schematic representation of the synthesis of mesoporous silica nanorods (Gd-Dye@MSN-R).

24 h. The as-synthesized nanorods were collected by centrifugation. After washing with water and ethanol, the nanorods were redispersed in acidic ethanol and the mixture was heated at 60°C for 24 h to remove the surfactant. Finally, the surfactant-free nanorods, termed Dye@MSN-R, were mixed with $GdCl_3{\cdot}6H_2O$ (10 mg) in 75% aqueous methanol (80 mL) and stirred at 40°C for 18 h to form the multifunctional nanorods Gd-Dye@MSN-R. (Detailed synthetic procedures are described in the Supporting Information.) The amount of Gd^{3+} in Gd-Dye@MSN-R was determined by inductively coupled plasma mass spectrometric analysis to be 0.275 wt%, which is about 26 637 Gd atoms per rod. We also synthesized small Gd-Dye@MSN spheres (≈100 nm) by using less of the DTPA ligand in the co-condensation process (data on Gd-Dye@MSN-R are provided in the Supporting Information). However, their biological behavior is a subject for another report.

The morphology and size distribution of Gd-Dye@MSN-R were examined by transmission electron microscopy (TEM). Figure 1a and b show a representative rod shape and a higher-resolution image of the Gd-Dye@MSN-R, respectively. Statistical analysis of the TEM image for the aspect ratio of Gd-Dye@MSN-R (Figure 1c) indicates that the average width of the nanorod is about 107 ± 9.4 nm, and 78 % of the nanorods have an aspect ratio of 3 to 5. The textural properties were determined by nitrogen adsorption/desorption isotherms (Figure 1d and Table S1 in the Supporting Information) and X-ray diffraction (XRD, Figure 1e). The isotherms exhibit three sections: a steeply rising step at $P/P_0 = 0.3$–0.35, a large hysteresis at $P/P_0 =$ 0.5–0.6, and another steep one at $P/P_0 = 0.95$. The first rising step is due to the well-ordered mesoporous structure with a pore size of 2.2 nm, which corresponds to the three characteristic hexagonal packing peaks of the XRD spectrum. The second one is attributed to the disordered pores with a pore size larger than 3 nm, and the last one to the macropores formed from packing of the nanorods. A small number of pores collapsed after loading Gd^{3+} into the Dye@MSN-R; this is revealed by the decreased pore volume and the disordered XRD pattern (the solid and dashed lines in Figure 1d and e). Nevertheless, Gd-Dye@MSN-R probes still possess a high surface area of 1014 $m^2\,g^{-1}$ and a large pore volume of 0.788 $cm^3\,g^{-1}$. The maximal UV/Vis absorption and fluorescence emission bands are at 488 and 520 nm (excitation at 488 nm, see Supporting Information Figure S2a), respectively, similar to the free dye. However, the dye incorporated in Gd-Dye@MSN-R is more stable than the free dye.[15] Gd-Dye@MSN-R can be suspended well in water (Fig-

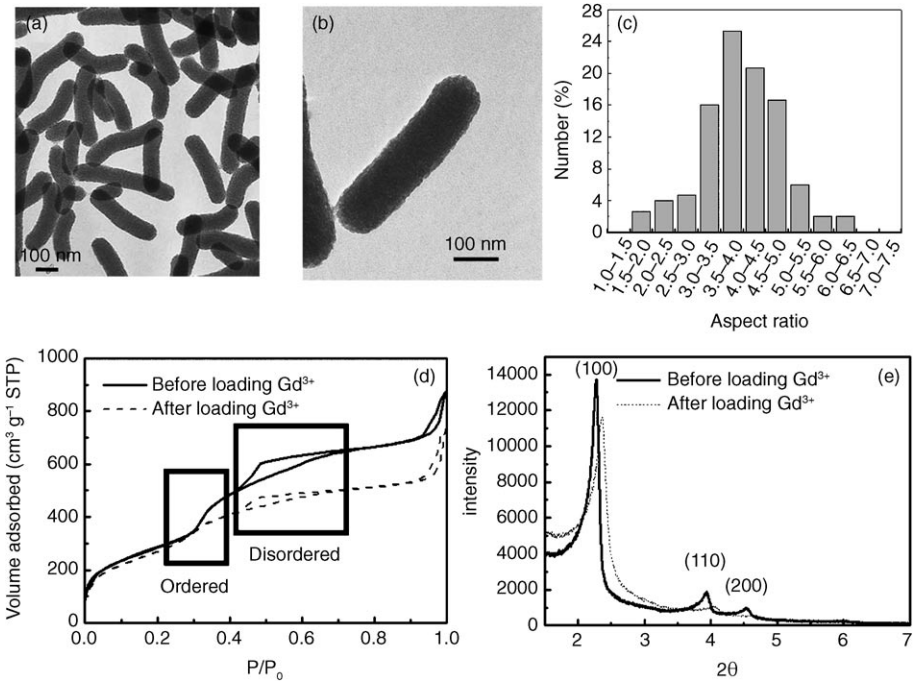

Figure 1. a) Low-resolution and b) high-resolution TEM images of Gd-Dye@MSN-R. c) Statistical analysis of TEM image for aspect ratio of Gd-Dye@MSN-R. d) Brunauer–Emmett–Teller (BET) nitrogen adsorption/desorption isotherms before and after loading of Gd^{3+} ions. The steeply rising step at $P/P_0 = 0.3$–0.35 is due to the ordered pores and the hysteresis at $P/P_0 = 0.5$–0.65 is due to the disordered pores. e) Powder XRD patterns before and after loading of Gd^{3+} ions.

ure S2b), and the uniform green fluorescence excited with a UV illuminator is shown in Figure S2c.

Another more important function of Gd-Dye@MSN-R is the MRI contrast-enhancing capability. We obtained the relaxivities of Gd-Dye@MSN-R with a Biospec spectrometer. By plotting $1/T_1$ and $1/T_2$ versus Gd^{3+} concentration, we obtained a good linear relationship (Figure 2a and b), with relaxivities of $r_1 = 22$ and $r_2 = 41$ мм$^{-1}$ s^{-1} at 0.47 T. These are about five and ten times higher, respectively, than the values for the complex $[Gd(DTPA)]^{2-}$. The high r_1 and r_2 values and the low r_2:r_1 ratio of 1.86 indicate that Gd-Dye@MSN-R could be used as a good dual-contrast agent for both T_1- and T_2-weighted imaging. In vitro T_1-weighted images, taken with a 4.7 T Biospec spectrometer (Figure 2c), show that the image lightens up faster than those of the corresponding Magnevist, thus indicating that Gd-Dye@MSN-R is a better T_1 contrast agent. On the other hand, the T_2-weighted image of Gd-Dye@MSN-R darkens faster than that of Magnevist. The relaxivity of the Gd^{3+}-based contrast agent is governed by several factors: the number of coordinated water molecules, the water exchange rate, and the tumbling rate.[11,24] For Gd-Dye@MSN-R, $[Gd(DTPA)]^{2-}$ is covalently bonded to the interior surface of the narrow pore of mesoporous silica. The confinement slows down the tumbling rate and consequently enhances the relaxivities.

To explore the possibility of utilizing the bifunctional properties of Gd-Dye@MSN-R in nanomedicine, we examined its function as a cell marker. 3T3-L1 mouse fibroblast cells were incubated with Gd-Dye@MSN-R (150 μg mL^{-1}) in serum-free medium (Dulbecco's modified Eagle's medium, DMEM) for different durations followed by quantification of the labeling efficiency by flow cytometry (see Supporting Information). After incubation for 30 min, 72% of cells were labeled with the nanorods, and the cell-labeling efficiency reached 99% after 2 h of incubation. We calculated that the uptake was about 3×10^3 Gd-Dye@MSN-R per 3T3-L1 cell for an incubation time of 1 h. We also treated the cells with different concentrations of Gd-Dye@MSN-R to find out the uptake saturation (see Supporting Information). An increase in the concentration of Gd-Dye@MSN-R resulted in a higher amount of nanorod cell uptake, and the saturated concentration of Gd-Dye@MSN-R was 300 μg mL^{-1} (99% of cells expressed fluorescence signals).

In Figure 3a, the confocal microscopy image shows that Gd-Dye@MSN-R was internalized into cells without any transfection agent and the nanorods aggregated inside the cell, as indicated by the nonuniform green fluorescent spots in the cytoplasm. The nanorods will also be engulfed by monocytes, such as RAW264.7, with excellent efficiency. Large micrometer-sized iron oxide nanoparticles have been reported to label immune cells in vivo.[27] Our results suggest that Gd-Dye@MSN-R could be used for labeling both phagocytic and nonphagocytotic cells without interference from a transfecting agent. Although the uptake efficiency may be increased in the presence of a transfecting agent, such as lipofectamine, MSN alone is sufficient; furthermore, one can avoid the cytotoxicity of lipofectamine with Gd-Dye@MSN-R alone (see below).

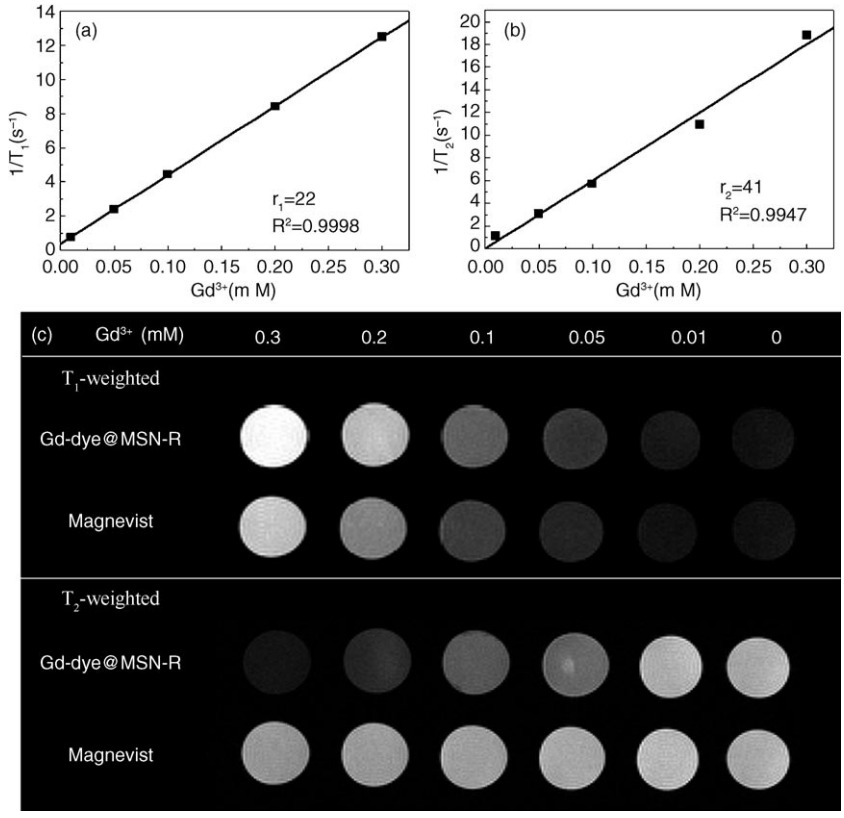

Figure 2. Plots of $[Gd^{3+}]$ (мм) versus a) $1/T_1$ and b) $1/T_2$ measured with a 0.47-T Biospec spectrometer. The slope is the relaxivity, r_1 or r_2. c) T_1- and T_2-weighted images of Gd-Dye@MSN-R and Magnevist at different Gd^{3+} concentrations, taken with a 4.7-T Biospec spectrometer.

In our previous work,[16] we demonstrated that cell internalization of fluorescent mesoporous silica nanoparticles (FITC-MSN) is energy dependent and could be suppressed by a clathrin inhibitor. This implies that the cell-uptake mechanism for the nanorods, which have similar surface properties to FITC-MSN, should involve clathrin-dependent endocytosis. The cells for MRI were prepared by incubating 1×10^5 cells with Gd-Dye@MSN-R (300 μg mL^{-1}) for 1 h followed by centrifugation to form pellets. The images were taken with a 1.5-T MRI system. The T_1-weighted image of the cells treated with Gd-Dye@MSN-R is significantly brighter (Figure 3b, right) compared to that of the untreated cells (Figure 3b, left), whereas in T_2-weighted magnetic reso-

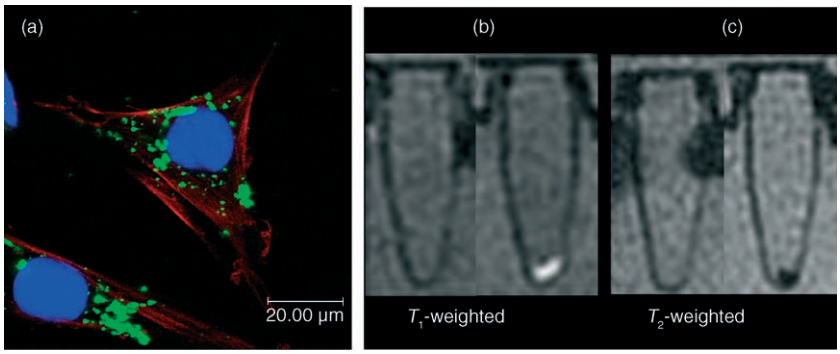

Figure 3. a) Confocal image of 3T3-L1 cellular uptake of Gd-Dye@MSN-R. b) T_1-weighted and c) T_2-weighted magnetic resonance images of a pellet of 1×10^5 cells treated with Gd-Dye@MSN-R for 1 h, taken with a 1.5-T magnetic resonance instrument. The left side in each set of images is untreated cells as a control.

nance mode the pellet treated with nanorods exhibits significant darkening of the image (Figure 3c).

Finally, the effects on cell viability and cell function, such as adipogenic differentiation of 3T3-L1 cells, were examined. 3-(4,5-Dimethylthiazol-2-yl)-2,5-diphenyltetrazolium bromide (MTT) assays (Figure 4a) showed that there is no adverse effect on cell viability, even at the very high concentration of 300 μg mL^{-1}. Adipogenic differentiation with the formation and accumulation of lipid vacuoles was examined. Cells were incubated with Gd-Dye@MSN-R (300 μg mL^{-1}) for 1 h followed by washing with phosphate-buffered saline (PBS), and then cultured in adipogenic medium for 14 days, fixed with 4% formaldehyde, and stained with oil-red O. As shown in Figure 4b and c, adipogenic differentiation of 3T3-L1 was only observed in cells grown in adipogenic medium, not in regular growth medium, and there is no difference between nanorod-treated and untreated cells (Figure 4d and e).

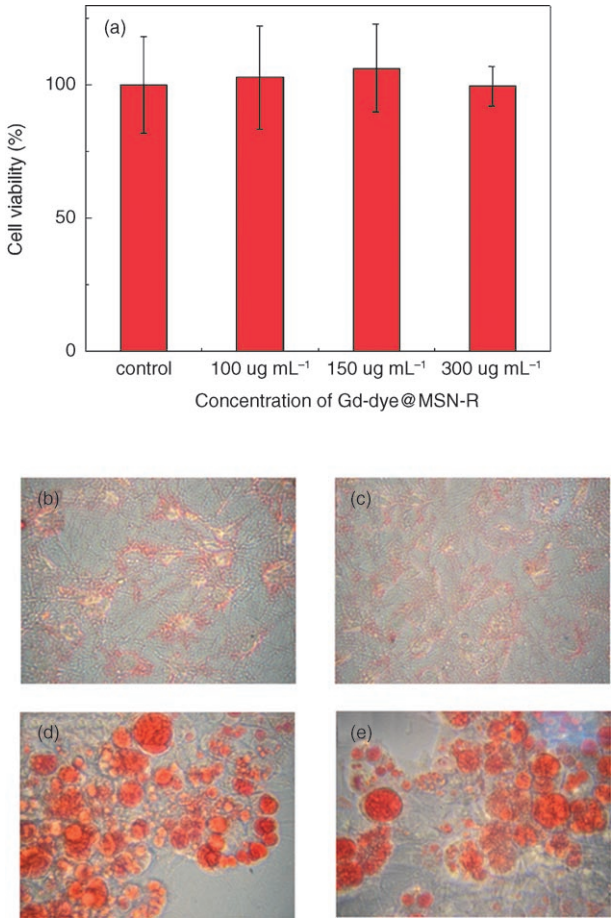

Figure 4. a) MTT assay of 3T3-L1 cells incubated with different amounts of Gd-Dye@MSN-R. 3T3-L1 cells were first treated with b,d) vehicle or c,e) Gd-Dye@MSN-R (300 μg mL^{-1}) for 1 h and then incubated with b,c) regular growth medium as negative control or d,e) adipogenic medium for differentiation. Original magnification, × 200. The images represent two independent experiments.

In summary, a versatile multifunctional mesoporous nanoprobe (Gd-Dye@MSN-R) with fluorescence and paramagnetism has been successfully developed. The nanorods display high relaxivities and can serve as either a T_1 or T_2 MRI contrast agent. Since most nanoprobes have only T_2-enhancing capability, the T_1 function is significant in cell tracking. Gd-Dye@MSN-R also showed good biocompatibility, exhibiting no short-term cytotoxicity and high cell-uptake efficiency without any transfection agent. In our previous work, we showed that the mesoporous silica nanoparticles eventually docked in the liver and spleen,[28] and then could excrete through the liver, bile, and intestines.[29] The metal ion is not limited to Gd; other metal ions, such as ^{111}In and ^{64}Cu, could be incorporated for nuclear medicine applications. This multifunctional nanomaterial has great potential in monitoring cell trafficking and cancer cell metastasis, and drug/DNA delivery.

Experimental Section

Synthesis of multifunctional mesoporous silica nanorods (Gd-Dye@MSN-R): Fluorescein isothiocyanate (FITC; 0.5 mg) and 3-aminopropyltrimethoxysilane (APTMS; 49 μL) were stirred in ethanol (99%, 2.5 mL) to form FITC-APTMS. 2-(4-Isothiocyanatobenzyl)diethylenetriaminepentaacetic acid (DTPA-ph-NCS; 20 mg) and APTMS (49 μL) were stirred in nanopure water (2.5 mL), and the pH of the solution was adjusted to 9.5–10 by adding 1N $NaOH_{(aq)}$ to form DTPA-ph-NCS-APTMS. Both solutions were prepared in advance and were stirred at room temperature for 24 h. CTAB (0.58 g, 1.64×10^{-3} mole) and an ethanol solution (0.226 M, 5 mL) of TEOS were dissolved in aqueous ammonia solution (0.51 M, 300 mL). The stock solution was stirred at 50°C for 5 h. FITC-APTMS, DTPA-ph-NCS-APTMS, and an ethanol solution (1.13 M, 5 mL) of TEOS were added with vigorous stirring for 1 h. The solution was then aged statically at 50°C for

24 h. As-synthesized samples were collected by centrifugation and washed with nanopure water and ethanol several times. The CTAB surfactant was removed by heating in acidic ethanol (1 g HCl in 50 mL ethanol) at 60°C for 24 h followed by centrifugation and washing with ethanol and nanopure water. The Gd^{3+}-unloaded mesoporous silica nanorods (Dye@MSN-R, 250 mg) were redispersed in 75% aqueous methanol (80 mL) containing $GdCl_3 \cdot 6H_2O$ (10 mg) and stirred at 40°C for 18 h. The unchelated Gd^{3+} ions were removed by washing with aqueous HCl solution (pH = 5). The supernatant in each washing was checked with a sodium acetate buffer solution of xylenol orange (pH = 5.5) to ensure the unchelated Gd^{3+} ions were removed completely.

Cell uptake: 3T3-L1 mouse fibroblast cells were seeded at 1×10^5 cells in high-glucose DMEM supplemented with 10% fetal bovine serum (FBS) in a 12-well plate. The culture was kept at 37°C in an atmosphere of 5% CO_2 and 95% air. After cell attachment for 24 h, the cells were incubated with 100, 150, or 300 μg Gd-Dye@MSN-R in serum-free medium (1 mL) for 0.5–3 h, washed with medium twice, and then further incubation in serum-containing medium was carried out for 24 h.

Confocal microscopy: The cell-uptake procedure was carried out as previously described, followed by washing with PBS several times and fixing with 4% paraformaldehyde at room temperature for 10 min. The cells were washed with PBS three times and incubated with 0.2% Triton X-100 and then 3% bovine serum albumin in PBS for 5 and 30 min, respectively. Rhodamine phalloidin was used for staining the filamentous actin skeleton at room temperature for 20 min. The nucleus was stained with 4′,6-diamidino-2-phenylindole (2 μg mL^{-1}) in H_2O for 5 min.

MTT assay: 3T3-L1 mouse fibroblast cells were seeded at 4500 cells in high-glucose DMEM supplemented with 10% FBS in a 96-well plate. The culture was kept at 37°C in an atmosphere of 5% CO_2 and 95% air. After cell attachment for 24 h, the cells were incubated with 100, 150, or 300 μg Gd-Dye@MSN-R in serum-free medium (1 mL) for 2 h and washed with medium twice. Regular medium (20 μL) and MTT (20 μL) in PBS buffer (5 mg mL^{-1}) were added followed by further incubation. After 4 h, DMSO (160 μL) was added to dissolve the purple formazan product, which was formed from the reduction of MTT in the mitochondria of living cells, and then the absorbance was measured at 570 nm by an enzyme-linked immunosorbent assay reader (Bio-Rad).

Cell differentiation: The effects of Gd-Dye@MSN-R uptake on cellular differentiation were examined as follows. To induce adipogenic differentiation, 3T3-L1 cells were first incubated with Gd-Dye@MSN-R (300 μg mL^{-1}) for 1 h followed by a PBS wash and then cultured in adipogenic medium or regular growth medium for 14 days. Medium changes were carried out twice weekly. Adipogenic medium consisted of high-glucose DMEM supplemented with isobutyl-1-methylxanthine (0.5 mM, Sigma–Aldrich), dexamethasone (1 μM, Sigma–Aldrich), insulin (10 ng mL^{-1}, Sigma–Aldrich), indomethacin (50 μM, Sigma–Aldrich), and 10% FBS. Adipogenic differentiation was assessed by the cellular accumulation of neutral lipid vacuoles after cells were fixed with 4% formaldehyde and stained with oil-red O (Sigma–Aldrich).

Keywords:
fluorescent probes · imaging · magnetic properties · mesoporous materials · nanorods

[1] M. Mimeault, S. K. Batra, *Stem Cells* **2007**, *24*, 2319–2345.
[2] K. L. Knutson, W. Wagner, M. L. Disis, *Cancer Immunol. Immunother.* **2006**, *55*, 96–103.
[3] S. Kim, Y. T. Lim, E. G. Soltesz, A. M. De Grand, J. Lee, A. Nakayama, J. A. Parker, T. Mihaljevic, R. G. Laurence, D. M. Dor, L. H. Cohn, M. G. Bawendi, J. V. Frangioni, *Nat. Biotechnol.* **2004**, *22*, 93–97.
[4] D. R. Larson, W. R. Zipfel, R. M. Williams, S. W. Clark, M. P. Bruchez, F. W. Wise, W. W. Webb, *Science* **2003**, *300*, 1434–1436.
[5] X. Michalet, F. F. Pinaud, L. A. Bentolila, J. M. Tsay, S. Doose, J. J. Li, G. Sundaresan, A. M. Wu, S. S. Gambhir, S. Weiss, *Science* **2005**, *307*, 538–544.
[6] P. K. Chattopadhyay, D. A. Price, T. F. Harper, M. R. Betts, J. Yu, E. Gostick, S. P. Perfetto, P. Goepfert, R. A. Koup, S. C. De Rosa, M. P. Bruchez, M. Roederer, *Nat. Med.* **2006**, *12*, 972–977.
[7] I. Brigger, C. Dubernet, P. Couvreur, *Adv. Drug Delivery Rev.* **2002**, *54*, 631–651.
[8] A. Dzik-Jurasz, *Br. J. Radiol.* **2004**, *77*, 296–307.
[9] R. Weissleder, U. Mahmood, *Radiology* **2001**, *219*, 316–333.
[10] S. Aime, C. Carrera, D. D. Castelli, S. G. Crich, E. Terreno, *Angew. Chem* **2005**, *117*, 1847–1849; *Angew. Chem. Int. Ed.* **2005**, *44*, 1813–1815.
[11] V. C. Pierre, M. Botta, K. N. Raymond, *J. Am. Chem. Soc.* **2005**, *127*, 504–505.
[12] E. Tóth, R. D. Bolskar, A. Borel, G. González, L. Helm, A. E. Merbach, B. Sitharaman, L. J. Wilson, *J. Am. Chem. Soc.* **2005**, *127*, 799–805.
[13] X. Wen, E. F. Jackson, R. E. Price, E. E. Kim, Q. P. Wu, S. Wallace, C. Charnsangavej, J. G. Gelovani, C. Li, *Bioconjugate Chem.* **2004**, *15*, 1408–1415.
[14] Y. H. Liu, H. P. Lin, C. Y. Mou, *Langmuir* **2004**, *20*, 3231–3239.
[15] Y. S. Lin, C. P. Tsai, H. Y. Huang, C. T. Kuo, Y. Hung, D. M. Huang, Y. C. Chen, C. Y. Mou, *Chem. Mater.* **2005**, *17*, 4570–4573.
[16] D. M. Huang, Y. Hung, B. S. Ko, S. C. Hsu, W. H. Chen, C. L. Chien, C. P. Tsai, C. T. Kuo, J. C. Kang, C. S. Yang, C. Y. Mou, Y. C. Chen, *FASEB J.* **2005**, *19*, 2014–2016.
[17] C. Y. Lai, B. G. Trewyn, D. M. Jeftinija, K. Jeftinija, S. Xu, S. Jeftinija, V. S. Y. Lin, *J. Am. Chem. Soc.* **2003**, *125*, 4451–4459.
[18] D. R. Radu, C. Y. Lai, J. W. Wiench, M. Pruski, V. S. Y. Lin, *J. Am. Chem. Soc.* **2004**, *126*, 1640–1641.
[19] J. Lu, M. Liong, J. I. Zink, F. Tamanoi, *Small* **2007**, *3*, 1341–1346.
[20] Y. S. Lin, S. H. Wu, Y. Hung, Y. H. Chou, C. Chang, M. L. Lin, C. P. Tsai, C. Y. Mou, *Chem. Mater.* **2006**, *18*, 5170–5172.
[21] F. Torney, B. G. Trewyn, V. S. Y. Lin, K. Wang, *Nat. Nanotechnol.* **2007**, *2*, 295–300.
[22] O. Veiseh, C. Sun, J. Gunn, N. Kohler, P. Gabikian, D. Lee, N. Bhattarai, R. Ellenbogen, R. Sze, A. Hallahan, J. Olson, M. Zhang, *Nano Lett.* **2005**, *5*, 1003–1008.
[23] H. Yang, S. Santra, G. A. Walter, P. H. Holloway, *Adv. Mater.* **2006**, *18*, 2890–2894.
[24] S. Santra, R. P. Bagwe, D. Dutta, J. T. Stanley, G. A. Walter, W. Tan, B. M. Moudgil, R. A. Mericle, *Adv. Mater.* **2005**, *17*, 2165–2169.
[25] W. J. M. Mulder, R. Koole, R. J. Brandwijk, G. Storm, P. T. K. Chin, G. J. Strijkers, C. D. Donega, K. Nicolay, A. W. Griffioen, *Nano Lett.* **2006**, *6*, 1–6.
[26] W. J. Rieter, J. S. Kim, K. M. L. Taylor, H. An, W. Lin, T. Tarrant, W. Lin, *Angew. Chem.* **2007**, *119*, 3754–3756; *Angew. Chem. Int. Ed.* **2007**, *46*, 3680–3682.

[27] Y. L. Wu, Q. Ye, L. M. Foley, T. K. Hitchens, K. Sato, J. B. Williams, C. Ho, *Proc. Natl. Acad. Sci. USA* **2006**, *103,* 1852–1857.
[28] S. H. Wu, Y. S. Lin, Y. Hung, Y. H. Chou, Y. H. Hsu, C. Chang, C. Y. Mou, *ChemBioChem*, **2008**, *9*, 53–57.
[29] H. S. Choi, W. Liu, P. Misra, E. Tanaka, J. P. Zimmer, B. I. Ipe, M. G. Bawendi, J. V. Frangioni, http://www.nature.com/nbt/journal/v25/n10/full/nbt1340.html, *Nat. Biotechnol.* **2007**, *25*, 1165–1170

Received: June 28, 2007
Revised: October 27, 2007
Published online on January 18, 2008

